On Frame Synchronization in Aeronautical Telemetry

MICHAEL RICE, Senior Member, IEEE
Brigham Young University
Provo, UT, USA

ANDREW MCMURDIE
Raytheon Missile Systems
Tucson, AZ, USA

Frame synchronizers, suitable for use with continuous phase modulation (CPM) in the presence of phase and frequency offsets, are derived for periodically inserted preamble bits in continuous-mode transmission. The resulting frame synchronizers involve single or double correlations of the received samples with a local copy of the CPM samples corresponding to the preamble bits. Of particular interest in aeronautical telemetry is shaped offset QPSK, telemetry group version (SOQPSK-TG), with the preamble defined in the integrated network enhanced telemetry (iNET) standard. Two low-complexity versions that leverage the special properties of the iNET preamble and SOQPSK-TG operating at 2 samples/bit are developed. Simulation results show that most frame synchronizers are capable of achieving acceptable performance for $E_b/N_0 \geq 0$ dB and the maximum frequency offset that can be tolerated increases with E_b/N_0 to about 3% of the bit rate.

Manuscript received June 25, 2015; revised January 8, 2015, April 18, 2016; released for publication May 30, 2016.

DOI. No. 10.1109/TAES.2016.150439.

Refereeing of this contribution was handled by L. Kaplan.

This work was funded by the Test Resource Management Center Test and Evaluation Science and Technology Program through the U. S. Army Program Executive Office for Simulation, Training and Instrumentation under Contract W900KK-13-C-0026 (PAQ).

Authors' addresses: M. Rice, Department of Electrical & Computer Engineering, Brigham Young University, 459 Clyde Building, Provo, UT 84602; A. McMurdie, Raytheon Missile Systems, 1151 E. Hermans Rd, Tucson, AZ 85756. Corresponding author is M. Rice, E-mail: (mdr@byu.edu).

I. INTRODUCTION

The traditional aeronautical telemetry link is a continuous-mode, one-way downlink from an airborne test article to a ground-based receiver. The recently introduced standard for a networked version of aeronautical telemetry, called iNET for integrated network enhanced telemetry [1], defines packetized transmission in which the preamble and attached sync marker (ASM) fields precede the data field. As of this writing, there is interest in periodically inserting the iNET preamble and ASM fields into continuous-mode links to enable data-aided estimators for synchronization, equalization, and channel quality monitoring. A prerequisite to enabling the data-aided estimators is identification of the start of the preamble in the received signal. Following the terminology most often used in the open literature, we refer to finding the start of the preamble as frame synchronization. Because the received signal corresponding to the preamble and ASM fields is to be used to estimate such things as timing, frequency, and phase offsets, frame synchronization must be performed in the presence of these offsets. Furthermore, frame synchronization must function with continuous phase modulation (CPM) as described in Section II.

Most previously published work on frame synchronization has been devoted to linear modulation. The usual approach is to start with symbol-synchronous matched filter outputs of the form

$$r_k = e^{j\theta} e^{j\omega k} a_k + z_k \tag{1}$$

where a_k is the kth symbol drawn from a constellation $\mathcal{A}$; θ and ω are the phase and frequency offsets, respectively; and z_k is a sample of the additive noise. The basic idea is to find the starting point of a known word (whose elements are members of $\mathcal{A}$) based on observing r_k. For $\theta = \omega = 0$ in (1), the intuitive approach is to correlate the sequence r_k with a locally stored copy of the known word. Barker [2] was the first to describe the use of a correlator for binary phase shift keying (BPSK), i.e., $a_k \in \{-1, +1\}$. Massey [3] derived the maximum likelihood (ML) frame synchronizer for the same case. The ML frame synchronizer comprised Barker's correlator and a nonlinear correction term to account for the random data preceding and following the known word. Simulation results presented by Nielsen [4] showed that the ML frame synchronizer achieves significant improvement over the simple correlator. Chiani [5] derived the ML synchronizer for BPSK for $\omega = 0$, $\theta \neq 0$. The problem was formulated as a likelihood ratio test based on the marginalized probability density function of r_k, assuming θ to be a uniform random variable on the interval $[-\pi, \pi)$ and assuming uniformly distributed data symbols. The result involved a noncoherent correlation followed by a correction term. Generalizations to M-ary phase shift keying (MPSK) for $M > 2$ were also discussed. Lui and Tan [6] generalized Massey's ML result [3] to nonbinary quadrature amplitude modulation (QAM). Both the coherent case, $\theta = \omega = 0$ in (1), and the noncoherent case,

$\omega = 0, \theta \neq 0$ in (1), were examined. For the coherent case, the ML frame synchronizer is a correlator with a data correction term. For the noncoherent case, θ was assumed to be a uniform random variable on the interval $[-\pi, \pi)$, and the corresponding ML frame synchronizer was derived from the marginalized probability density function of r_k. The resulting frame synchronizer comprises a form of noncoherent correlation and a data correction term. Chiani and Martini [7] derived analytical expressions bounding the false alarm and miss probabilities of the Lui and Tan approach [6], and Bastaki et al. [8] extended the work of Lui and Tan [6] to the observation of multiple frames.

For the case in (1), where $\omega \neq 0$, frame synchronization must be performed in the presence of a frequency offset. Three basic approaches have been used to deal with the frequency offset. The first, published by Choi and Lee [9] and devoted to MPSK, assumed θ and ω are independent uniform random variables on $[-\pi, \pi)$ and derived the ML frame synchronizer from the marginalized probability density function of r_k. The result was a double correlator replacing the traditional correlator and a data correction term. The second approach, from Koo and Lee [10], incorporated the unknown phase and frequency in a joint estimation problem. A three-step process was described involving estimates of θ and ω for each possible starting location, followed by maximization over the starting locations. The third approach, described by Pedone et al. [11], is based on a novel stepwise (or stepwise) approximation of the phase ramp because of the frequency offset. The result is a partition of the required correlations into coherent and noncoherent segments.

Notable variations on the problem include "one shot" estimators for burst-mode communications [12], the closely related problem of variable length frames [13, 14], and the case in which the known word is distributed through the data [15, 16].

Because aeronautical telemetry uses CPM, the model for the observed random variables is different from (1). Whereas considerable attention has been devoted to the frame synchronization problem for linear modulations, only a few publications have tackled the problem for CPM. Stantchev and Fettweis [17] developed the ML frame synchronizer for noncoherent M-ary frequency shift keying (FSK) based on the magnitudes of the M-matched filter outputs. For the special case of $M = 4$, Bobula et al. [18] devised an ad hoc frame synchronization technique based on the sign of limiter-discriminator outputs. Both approaches leveraged the special properties of orthogonal FSK, and neither easily generalizes to arbitrary CPM. Huh and Krogmeier [19] modeled the observed symbols as noisy Markov chain outputs and derived frame synchronizers with excellent performance. Their approach was general, with application to both linear modulations with memory (e.g., coded modulation) or CPM, but considered only additive white Gaussian noise (AWGN) with $\theta = \omega = 0$. Hosseini and Perrins [20] discussed the problem of one-shot frame synchronization for CPM based on a clever preamble design described in [21]. The result was a double correlator similar to that of Choi and Lee [9] and including a term that accounted for the noise-only measurements preceding the burst.

In this paper, we return to basic principles and revisit the problem of frame synchronization for CPM for continuous-mode transmission with a periodically inserted known word and in the presence of phase and frequency offsets and AWGN. After identifying suitable approximations, we follow the approaches of both Choi and Lee [9] and Pedone et al. [11] in dealing with the frequency offset. We show that correlation-type functions both with and without correction terms operating on samples of the received waveform and samples of the waveform corresponding to the known word follow from the analysis. Finally, by leveraging the particular properties of shaped offset QPSK, telemetry group version (SOQPSK-TG) and the iNET preamble, we develop low-complexity frame synchronizers whose performance is comparable to that of their full-complexity counterparts. Some initial simulation results using a subset of these frame synchronizers over mulitpath channels are described by the authors in [22].

This paper is organized as follows. A detailed problem formulation is described in Section II. In Section III, eight frame synchronizers that follow from the problem formulation are described, together with two low-complexity counterparts that leverage the special properties of the iNET preamble and SOQPSK-TG operating at 2 samples/bit. The performance of these frame synchronizers is outlined in Section IV, followed by the conclusions and a short discussion in Section V. The frame synchronizers described in Section III are derived in Appendices A and B. In these sections, boldface variables denote column vectors and $(\cdot)^\top$ denotes the transpose operation.

II. PROBLEM FORMULATION

The bit sequence used to create the CPM waveform is illustrated in Fig. 1a. The motivation for this particular structure is the iNET standard from aeronautical telemetry [1], but the generalization to other word fields is straightforward. The bits are used to modulate a CPM carrier, whose continuous-time complex-valued low-pass equivalent representation is [23–25]

$$s_c(t) = \exp\{j\phi(t)\} \tag{2}$$

where

$$\phi(t) = 2\pi \int_{-\infty}^{t} \sum_k h_k a_k g(x - kT_s)\, dx. \tag{3}$$

Here, a_k is the kth symbol, h_k is the modulation index applied during the kth symbol interval, T_s is the symbol interval, and $g(t)$ is the frequency pulse, spanning L_g symbol times and normalized to have area 1/2. Three forms of CPM are defined in the aeronautical telemetry standard IRIG 106 [26]:

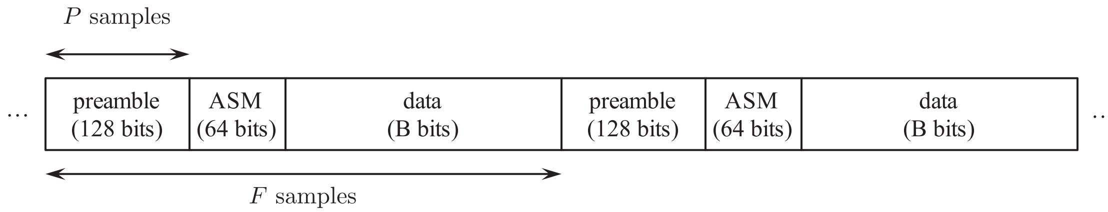

(a)

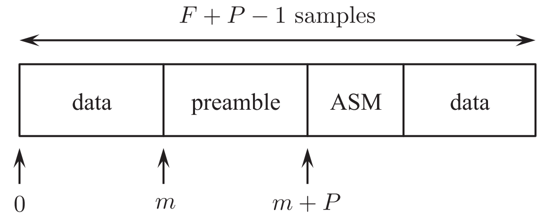

(b)

Fig. 1. Frame structure: (a) diagram illustrating periodic insertion of L_p preamble bits every L_f bits. Note relationship between bits and waveform samples. (b) Possible arrangement of P waveform samples corresponding to preamble bits in block of F samples.

- PCM/FM (for pulse code modulation with frequency modulation) is defined as follows:
  - $a_k \in \{-1, +1\}$
  - $T_s = T_b$, where T_b is the bit interval
  - $h_k = 0.7$ for all k
  - $g(t)$ is the length-2 raised cosine pulse [23–25]
- SOQPSK-TG is defined as follows:
  - a_k is drawn from a constrained ternary alphabet, as described in [27, 28]
  - $T_s = \mathrm{T}_b$
  - $h_k = 1/2$ for all k
  - $g(t)$ is a pulse spanning 8 bit times, as described in [27, 28]
- ARTM CPM (for advanced range telemetry CPM)
  - $a_k \in \{-3, -1, +1, +3\}$
  - $T_s = 2T_b$
  - $h_k = 4/16$ for k even and $h_k = 5/16$ for k odd
  - $g(t)$ is the length-3 raised cosine pulse [23–25]

The received signal is given by

$$r_c(t) = e^{j\theta} e^{j2\pi\nu t} s_c(t) + z_c(t) \tag{4}$$

where θ is the phase offset, ν is the frequency offset in cycles per second, and $z_c(t)$ is the thermal noise, modeled as a complex-valued circularly symmetric wide-sense stationary Gaussian random process with zero mean and autocorrelation

$$\mathrm{E}\left\{z_c\left(t+\tau\right) z_c^*\left(t\right)\right\} = 2N_0\delta\left(\tau\right). \tag{5}$$

In preparation for sampling at a rate of $1/T$ samples/s (equivalent to $N = T_b/T$ samples/bit), the received signal is filtered by an antialiasing filter. We assume the antialiasing filter is an ideal low-pass filter with bandwidth $1/2T$ and that the sample rate is sufficiently high so as not to produce noticeable aliasing in the spectrally shifted version of the CPM waveform $s_c(t)e^{j2\pi\nu t}$. The nth sample of the resulting sample sequence is given by

$$r(nT) = e^{j\theta} e^{j\omega n} e^{j\phi(nT)} + z(nT) \tag{6}$$

where $\omega = 2\pi\nu T$ rads/sample and $z(nT)$ is a sequence of uncorrelated complex-valued Gaussian random variables with zero mean and variance $2\sigma^2 = 2N_0/T$.

We assume continuous-mode transmission with an L_p-bit preamble sequence periodically inserted every $L_f - L_p$ bits to produce a frame with a length of L_f bits. The situation is illustrated in Fig. 1a for framed transmissions using the iNET frame structure [1]. Assuming a sample rate of N samples/bit, the problem may be restated in terms of samples: $P = NL_p$ samples, corresponding to the CPM waveform modulated by the preamble bits, are periodically inserted every $N(L_f - L_p)$ samples to produce a frame comprising $F = NL_f$ samples. Because the frame length is fixed and known, continuous transmission means that the preamble samples are guaranteed to be present in any contiguous block of F samples of the received signal. If the start of the preamble samples is assumed to be m and $m \in \{0, 1, \ldots, F-1\}$, then a block of $F + P - 1$ consecutive samples of the received signal must be available [19]. The concept is illustrated in Fig. 1b.

For notational convenience, we stack the $F + P - 1$ observed samples in the $(F + P - 1) \times 1$ vector

$$\mathbf{r} = \left[\, r\left(0\right) \quad r\left(T\right) \quad \cdots \quad r\left(\left(F+P-2\right)T\right) \right]^\top \tag{7}$$

and let

$$\mathbf{p} = \left[\, p\left(0\right) \quad p\left(T\right) \quad \cdots \quad p\left(\left(P-1\right)T\right) \right]^\top \tag{8}$$

be the $P \times 1$ vector of samples of the CPM waveform corresponding to the preamble bits. Let $\phi_m(nT)$ for $n = 0, 1, \ldots, F + P - 2$ be the sequence of phase samples corresponding to the case in which the preamble samples start at index m. Assuming the preamble samples occur only once in the block of $F + P - 1$ samples, the elements of $\phi_m(nT)$ are arranged as follows:

$$\underbrace{\phi_m(0)\cdots\phi_m((m-1)T)}_{\text{random data samples}} \times \underbrace{\phi_m(mT)\cdots\phi_m((m+P-1)T)}_{\text{preamble samples}} \times \underbrace{\phi_m((m+P)T)\cdots\phi_m((F+P-2)T)}_{\text{random data samples}}. \quad (9)$$

With this notation, we have $p(kT) = e^{j\phi_m((m+k)T)}$ for $k = 0, \ldots, P-1$. Consequently, under the hypothesis the preamble sequence begins at index m, the model for the received samples is

$$r(nT) = \begin{cases} e^{j\theta}e^{j\omega n}e^{j\phi_m(nT)} + z(nT) & 0 \le n < m \\ e^{j\theta}e^{j\omega n}p((n-m)T) + z(nT) & m \le n < m+P \\ e^{j\theta}e^{j\omega n}e^{j\phi_m(nT)} + z(nT) & m+P \le n < F+P-1. \end{cases} \quad (10)$$

Let $f(\mathbf{r}|m)$ be the conditional probability density function of the vector $\mathbf{r}$ given that the preamble samples start at index m. The ML frame synchronizer produces the decision

$$\hat{m} = \underset{0\le m\le F-1}{\operatorname{argmax}} \{f(\mathbf{r}|m)\}. \quad (11)$$

The difficulty lies in computing a usable form for $f(\mathbf{r}|m)$ from the conditional probability density function

$$f(\mathbf{r}|m,\theta,\omega,\phi_d) = \prod_{n=0}^{F+P-2} \frac{1}{2\pi\sigma^2} \exp\left\{-\frac{1}{2\sigma^2}\left|r(nT) - e^{j\theta}e^{j\omega n}e^{j\phi(nT)}\right|^2\right\} \quad (12)$$

where the vector

$$\phi_d = \left[\phi(0)\cdots\phi((m-1)T)\ \ \phi((m+P)T)\ \cdots\phi((F+P-2)T)\right]^\top \quad (13)$$

represents the phase samples corresponding to random data bits. Here, the phase, frequency, and random data are nuisance parameters.

We follow two approaches in dealing with the nuisance parameters and compare their performance. The first approach follows that of Choi and Lee [9] and is detailed in Appendix A. The second approach follows Pedone et al. [11] and is detailed in Appendix B. Each approach is based on a number of assumptions about the nuisance parameters. These assumptions are spelled out at the beginning of each appendix.

The derivations in both appendices rely on the following high-level assumptions:

1) The samples with the ASM bits are treated as part of the random data. In other words, the CPM samples with the ASM bits are not used for frame synchronization. This omission is motivated by the complexity reduction techniques associated with the repetitive structure of the preamble bits, as described in Section III.B. Frame synchronization performance improves if the ASM bits are used for frame synchronization. But this performance improvement is achieved at the expense of computational complexity.

2) In the block of $F + P - 1$ received samples, the preamble samples are assumed to occur only once, even though the block may contain one entire occurrence of the preamble samples and part of another occurrence.

3) The first phase sample of the preamble sample sequence, $\phi_m(mT)$, is due only to the first preamble bit. This is clearly a coarse approximation, because for $L_g > 1$ (the case for all three IRIG 106 modulations), each phase sample is influenced by the phase state, defined by previous input symbols, and the correlative state, defined by the previous $L_g - 1$ symbols and $g(t)$. See [23–25] for more details. The assumption is made for mathematical convenience. To do otherwise leads to an intractable result or a torturously difficult form.

The simulation results presented in Section IV help assess the impact of these approximations.

III. ML FRAME SYNCHRONIZERS

The frame synchronizers considered in this section are of the form

$$\hat{m} = \underset{0\le m\le F-1}{\operatorname{argmax}} \{L_i(m)\} \quad (14)$$

where $L_i(m)$ derives from ML considerations described in the sections that follow. It is understood that frame synchronization is based on $L_i(\cdot)$ as described in [14].

A. Full-Complexity Synchronizers

The first synchronizer considered is the simple correlator operating on the samples as discussed in [5]:

$$L_0(m) = \left|\sum_{k=0}^{P-1} r((k+m)T)\,p^*(kT)\right|. \quad (15)$$

The absolute value is used to account for unknown phase rotations because of phase and frequency offsets. A closely related frame synchronizer is the heuristic function [5]

$$L_{0\mathrm{h}}(m) = \left|\sum_{k=0}^{P-1} r((k+m)T)\,p^*(kT)\right| - \sum_{n=m}^{m+P-1} |r(nT)|. \quad (16)$$

The heuristic function comprises the correlator of L_0 and a correction term. It is well known that these functions do not perform well in the presence of a frequency offset. They are included here to demonstrate the improvement realized by the more complicated functions that follow.

The next four frame synchronizers are based on the development outlined in Appendix A. The function that follows from ML principles based on the marginalized probability density function of the vector **r** is

$$L_1(m) = \sum_{i=1}^{P-1} \left[\left| \sum_{k=i}^{P-1} r^*((k+m)T)\, p(kT)\, r((k+m-i)T) \times p^*((k-i)T) \right| - \sum_{n=i+m}^{m+P-1} |r(nT)|\, |r((n-i)T)| \right]. \tag{17}$$

The first term on the right-hand side of (17) was dubbed a "double correlation" by Choi and Lee [9]. The second term plays the role of Massey's data correction term [3]. Whereas the Choi-Lee function [9] computed the double correlation on the matched filter outputs and a local copy of the preamble symbols [cf. (1)], the double correlation here operates on samples of the received waveform and a local copy of the samples corresponding to the preamble bits. In this regard, the result is almost the same as that from Hosseini and Perrins [20], except the correction term is different.

Following Choi and Lee [9], three simplifications are investigated. First, the data correction term in (17) may be eliminated:

$$L_2(m) = \sum_{i=1}^{P-1} \left| \sum_{k=i}^{P-1} r^*((k+m)T)\, p(kT) \times r((k+m-i)T)\, p^*((k-i)T) \right|. \tag{18}$$

Second, only the $i = 1$ term in (17) is used:

$$L_3(m) = \left| \sum_{k=1}^{P-1} r^*((k+m)T)\, p(kT)\, r((k+m-1)T) \times p^*((k-1)T) \right| - \sum_{n=1+m}^{m+P-1} |r(nT)|\, |r((n-1)T)|. \tag{19}$$

Finally, only the $i = 1$ term in (18) is used:

$$L_4(m) = \left| \sum_{k=1}^{P-1} r^*((k+m)T)\, p(kT)\, r((k+m-1)T) \times p^*((k-1)T) \right|. \tag{20}$$

Each of these reduces the computational complexity of frame synchronization but does so with a loss in performance. The complexity–performance tradeoff is examined in Section IV.

The next two frame synchronizers follow from the development in Appendix B. The function that follows from a high signal-to-noise ratio (SNR) approximation and ML principles is

$$L_5(m) = \sqrt{\Lambda_0(m) + \sum_{n=1}^{L_{\mathrm{PDI}}-1} \bar{\Lambda}_n(m)} - \sum_{n=m}^{m+P-1} |r(nT)| \tag{21}$$

where

$$\Lambda_0(m) = \sum_{i=0}^{L_{\mathrm{PDI}}-1} \left| \sum_{k=iL_{\mathrm{coh}}}^{(i+1)L_{\mathrm{coh}}-1} r((k+m)T)\, p^*(kT) \right|^2 \tag{22}$$

and

$$\bar{\Lambda}_n(m) = 2 \left| \sum_{i=0}^{L_{\mathrm{PDI}}-1-n} \sum_{k=(i+n)L_{\mathrm{coh}}}^{(i+n+1)L_{\mathrm{coh}}-1} r((k+m)T)\, p^*(kT) \times \sum_{k'=iL_{\mathrm{coh}}}^{(i+1)L_{\mathrm{coh}}-1} r^*\left((k'+m)T\right) p\left(k'T\right) \right|. \tag{23}$$

Here, L_{PDI} and L_{coh} are design parameters such that $P = L_{\mathrm{PDI}}\, L_{\mathrm{coh}}$ and are described later in this paragraph. In addition, $\lambda_0(m)$ is the sample-based version of the noncoherent postdetection integration (NCPDI) concept, a standard result in code division multiple access acquisition [29, 30], and $\bar{\Lambda}_n(m)$ is the sample-based version of the n-span differential postdetection integration (n-span DPDI) principle [11]. The NCPDI term partitions the correlation involving P consecutive samples of the received signal and the pilot samples into segments of length-L_{coh} coherent correlation and noncoherently combines the L_{PDI} coherent correlations (the subscript PDI refers to postdetection integration). This would seem to solve the problem for the phase and frequency offsets. Therefore, the last frame synchronizer we consider is based just on the NCPDI term $\Lambda_0(m)$:

$$L_6(m) = \sum_{i=0}^{L_{\mathrm{PDI}}-1} \left| \sum_{k=iL_{\mathrm{coh}}}^{(i+1)L_{\mathrm{coh}}-1} r((k+m)T)\, p^*(kT) \right|^2. \tag{24}$$

B. Reduced-Complexity Synchronizers

The eight frame synchronizers described in the previous section involve correlations between the samples of the received signal and a local copy of preamble samples. For each m, the correlation requires P multiply–accumulate operations (and quite a number more for the double correlation functions). For SOQPSK-TG and the iNET preamble, an interesting complexity-reducing technique is available. The 128-bit iNET preamble is the 16-bit sequence $\mathrm{CD98}_{\mathrm{hex}}$ repeated eight times [1, pp. 48]. A plot of the complex-valued samples of SOQPSK-TG for $N = 2$ samples/bit corresponding to the iNET preamble is shown in Fig. 2. The samples appear to be clustered about eight equally spaced points on the unit circle. This suggests a quantized version of the local copy of the preamble samples, where the quantized version comprises values only at ± 1, $\pm j$, and $(\pm 1 \pm j)/\sqrt{2}$. Let $\tilde{p}(nT)$ for $n = 0, \ldots, 255$ be the quantized version of $p(nT)$.

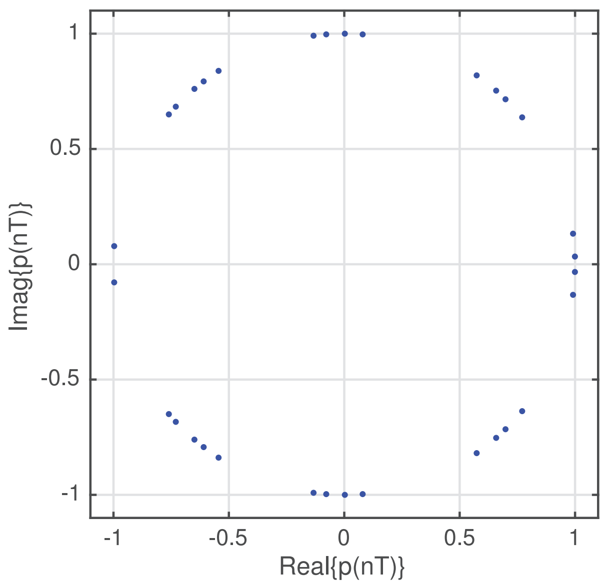

Fig. 2. Complex-valued samples of SOQPSK-TG, at sample rate of 2 samples/bit, corresponding to iNET preamble.

The reduction in computational complexity is best illustrated by considering the correlation

$$R(k) = \sum_{i=0}^{255} r((i+k)T)\, p^*(iT). \tag{25}$$

This correlation, based on the unquantized preamble samples, requires 256 complex-valued multiply–accumulate operations, which translates to 1024 real-valued multiplications and 1024 real-valued additions. Using $\tilde{p}(iT)$ (the quantized versions) in place of $p(iT)$ (the unquantized versions) all but eliminates the multiplications. If $r(nT) = r_R(nT) + jr_I(nT)$, the real and imaginary parts of $R(k)$ may be expressed as

$$\begin{aligned}\mathrm{Re}\{R(k)\} \approx & \sum_{i\in\mathcal{I}_1} r_R((i+k)T) - \sum_{i\in\mathcal{I}_2} r_R((i+k)T) \\ & + \sum_{i\in\mathcal{I}_3} r_I((i+k)T) - \sum_{i\in\mathcal{I}_4} r_I((i+k)T) \\ & + \frac{1}{\sqrt{2}}\Bigg[\sum_{i\in\mathcal{I}_5} r_R((i+k)T) - \sum_{i\in\mathcal{I}_6} r_R((i+k)T) \\ & + \sum_{i\in\mathcal{I}_7} r_I((i+k)T) - \sum_{i\in\mathcal{I}_8} r_I((i+k)T)\Bigg]\end{aligned} \tag{26}$$

and

$$\begin{aligned}\mathrm{Im}\{R(k)\} \approx & \sum_{i\in\mathcal{I}_1} r_I((i+k)T) - \sum_{i\in\mathcal{I}_2} r_I((i+k)T) \\ & - \sum_{i\in\mathcal{I}_3} r_R((i+k)T) + \sum_{i\in\mathcal{I}_4} r_R((i+k)T) \\ & + \frac{1}{\sqrt{2}}\Bigg[\sum_{i\in\mathcal{I}_5} r_I((i+k)T) - \sum_{i\in\mathcal{I}_6} r_I((i+k)T) \\ & - \sum_{i\in\mathcal{I}_7} r_R((i+k)T) + \sum_{i\in\mathcal{I}_8} r_R((i+k)T)\Bigg]\end{aligned} \tag{27}$$

respectively, where

$$\begin{aligned}\mathcal{I}_1 &= \{i, 0 \le i < 256 \mid \tilde{p}(iT) = +1\} \\ \mathcal{I}_2 &= \{i, 0 \le i < 256 \mid \tilde{p}(iT) = -1\} \\ \mathcal{I}_3 &= \{i, 0 \le i < 256 \mid \tilde{p}(iT) = +j\} \\ \mathcal{I}_4 &= \{i, 0 \le i < 256 \mid \tilde{p}(iT) = -j\} \\ \mathcal{I}_5 &= \left\{i, 0 \le i < 256 \mid \mathrm{Re}[\tilde{p}(iT)] = +1\big/\sqrt{2}\right\} \\ \mathcal{I}_6 &= \left\{i, 0 \le i < 256 \mid \mathrm{Re}[\tilde{p}(iT)] = -1\big/\sqrt{2}\right\} \\ \mathcal{I}_7 &= \left\{i, 0 \le i < 256 \mid \mathrm{Im}[\tilde{p}(iT)] = +1\big/\sqrt{2}\right\} \\ \mathcal{I}_8 &= \left\{i, 0 \le i < 256 \mid \mathrm{Im}[\tilde{p}(iT)] = -1\big/\sqrt{2}\right\}.\end{aligned} \tag{28}$$

This approach requires 512 real-valued additions and only 2 real-valued multiplications. The principle may be extended to the double correlation terms of (17)–(20) in a straightforward way.

Further complexity reductions are available for L_6. Because the preamble bit sequence comprises eight repetitions of the 16-bit pattern $\mathrm{CD98}_{\mathrm{hex}}$, the corresponding sample sequence is, to a first-order approximation, eight repetitions of the $Q = 16N$ sample sequence corresponding to the 16-bit sequence $\mathrm{CD98}_{\mathrm{hex}}$.[1] Let $q(nT)$ for $n = 0, \ldots, 16N - 1$ be this sequence. The relationship between the short sample sequence $q(nT)$ and the entire preamble sample sequence is illustrated in Fig. 3. In the figure, the start of the preamble sequence corresponds to the mth sample of the received signal. Thus, $r(mT)$ is aligned with both $p(0)$ and the first occurrence of $q(0)$. Q samples later, $r((m + Q)T)$ is aligned with $p(QT)$ and with the second occurrence of $q(0)$. And so on.

A remarkable reduction in computational complexity occurs with L_6 for $N = 2$ samples/bit. Here, the assignments $L_{\mathrm{coh}} = Q = 32$ and $L_{\mathrm{PDI}} = 8$ may be used. Recognizing that $\tilde{p}((\ell + 32i)T) = \tilde{q}(\ell T)$, L_6 becomes

$$L_{6q}(m) = \sum_{i=0}^{7} \left| \sum_{\ell=0}^{31} r((\ell + 32i + m)T)\, \tilde{q}^*(\ell T) \right|^2. \tag{29}$$

Using the quantized values for the short preamble sample sequences and collecting similar terms gives

$$L_{6q}(m) = \sum_{i=0}^{7} \left[I^2(m,i) + Q^2(m,i)\right] \tag{30}$$

[1] This is not quite true for the first Q-sample sequence because of the memory in SOQPSK-TG.

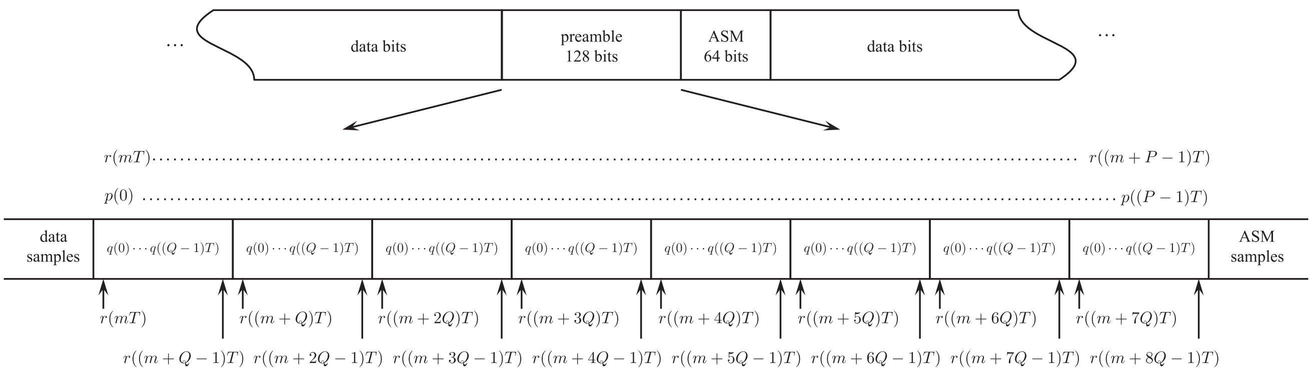

Fig. 3. Illustration of relationship between samples of received signal, samples of SOQPSK-TG signal corresponding to preamble, and samples of SOQPSK-TG signal corresponding to constituent bit sequence CD98_{hex}.

where

$$\begin{aligned} I(m,i) &\approx \sum_{i\in\mathcal{L}_1} r_R(\ell+32i+m) - \sum_{\ell\in\mathcal{L}_2} r_R(\ell+32i+m) \\ &+ \sum_{\ell\in\mathcal{L}_3} r_I(\ell+32i+m) - \sum_{\ell\in\mathcal{L}_4} r_I(\ell+32i+m) \\ &+ \frac{1}{\sqrt{2}}\left[\sum_{\ell\in\mathcal{L}_5} r_R(\ell+32i+m) - \sum_{\ell\in\mathcal{L}_6} r_R(\ell+32i+m)\right. \\ &\left. + \sum_{\ell\in\mathcal{L}_7} r_I(\ell+32i+m) - \sum_{\ell\in\mathcal{L}_8} r_I(\ell+32i+m)\right] \end{aligned} \tag{31}$$

and

$$\begin{aligned} Q(m,i) &\approx \sum_{\ell\in\mathcal{L}_1} r_I(\ell+32i+m) - \sum_{\ell\in\mathcal{L}_2} r_I(\ell+32i+m) \\ &- \sum_{\ell\in\mathcal{L}_3} r_R(\ell+32i+m) + \sum_{\ell\in\mathcal{L}_4} r_R(\ell+32i+m) \\ &+ \frac{1}{\sqrt{2}}\left[\sum_{\ell\in\mathcal{L}_5} r_I(\ell+32i+m) - \sum_{\ell\in\mathcal{L}_6} r_I(\ell+32i+m)\right. \\ &\left. - \sum_{\ell\in\mathcal{L}_7} r_R(\ell+32i+m) + \sum_{\ell\in\mathcal{L}_8} r_R(\ell+32i+m)\right] \end{aligned} \tag{32}$$

with

$$\begin{aligned} \mathcal{L}_1 &= \{0, 8, 16, 24\} \\ \mathcal{L}_2 &= \{4, 20\} \\ \mathcal{L}_3 &= \{2, 10, 14, 22\} \\ \mathcal{L}_4 &= \{6, 18, 26, 30\} \\ \mathcal{L}_5 &= \{1, 7, 9, 15, 17, 23, 25, 31\} \\ \mathcal{L}_6 &= \{3, 5, 11, 12, 13, 19, 21, 27, 28, 29\} \\ \mathcal{L}_7 &= \{1, 3, 9, 11, 12, 13, 15, 21, 23\} \\ \mathcal{L}_8 &= \{5, 7, 17, 19, 25, 27, 28, 29, 31\}. \end{aligned} \tag{33}$$

To further simplify the computation, it is straightforward to show that

$$\begin{aligned} I(m+32,i) &= I(m,i+1) \\ Q(m+32,i) &= Q(m,i+1) \end{aligned} \tag{34}$$

for $i = 0, 1, \ldots, 6$. The consequence of this relationship is that (30) may be computed by

$$\begin{aligned} L_{6q}(m) = L_{6q}(m-32) &- [I^2(m-32,0) + Q^2(m-32,0)] \\ &+ I^2(m,7) + Q^2(m,7) \end{aligned} \tag{35}$$

for $m \geq 32$. Thus, L_{6q} may be computed recursively, where each recursion requires four real-valued multiplications and 67 real-valued additions.

The performance penalty associated with equating L_{coh} to Q can be measured using the energy loss due to the phase rotation over the coherent correlation interval L_{coh}. The energy loss is proportional to $\text{sinc}^2(L_{\text{coh}}T\nu)$ [31], where ν is the continuous-time frequency offset; see (4). A plot of this loss versus the normalized frequency offset for SOQPSK-TG operating at $N = 2$ samples/bit is shown in Fig. 4. An energy loss of 1 dB occurs when the frequency offset is approximately 1.5% of the bit rate. The energy loss of 3 dB occurs at a frequency offset of 2.75% of the bit rate. This shows that as long as the frequency offset is on the order of 1% to 2% of the bit rate, the assignment $L_{\text{coh}} = Q$ has the potential to be a robust frame synchronizer.

A summary of the computational complexity, measured by the number of real-valued multiplication and square-root operations, is given in Table I for a normalized sample rate of $N = 2$ samples/bit. In the table, $L_{1q}(m)$ denotes (17), with $\tilde{p}(kT)$ replacing $p(kT)$. The quantized version of L_6 has clear advantages from a computational complexity point of view. The performance of these frame synchronizers is summarized in the next section.

IV. PERFORMANCE RESULTS

We evaluated the performance of the frame synchronizers L_0 through L_6 and the quantized version L_{6q} using computer simulation. The computer simulations followed the usual procedure: samples of an SOQPSK-TG

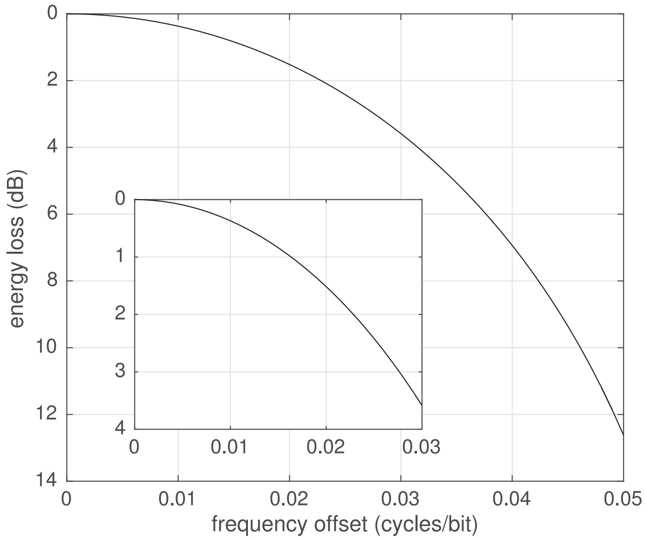

Fig. 4. Energy loss because of coherent correlation over interval $L_{\rm coh} = Q = 32$ samples as function of normalized frequency. These results correspond to $N = 2$ samples/bit.

TABLE I
Computational Complexity for Examined Frame Synchronizers for SOQPSK-TG with iNET Preamble and Operating at $N = 2$ Samples/Bit

Synchronizer	Multiplication	Square root
$L_0(m)$	1024	1
$L_{0\rm h}(m)$	1024	2
$L_1(m)$	424 320	511
$L_{1q}(m)$	163 200	511
$L_2(m)$	391 680	255
$L_3(m)$	3315	257
$L_4(m)$	3060	1
$L_5(m)$	1168	293
$L_6(m)$	1024	0
$L_{6\rm q}(m)$	4	0

signal operating at $N = 2$ samples/bit were created using a sequence of 1000 random data bits, the iNET preamble, the iNET ASM, and another sequence of 1000 random data bits. A frequency offset, equivalent to 0%, 1%, or 5% of the bit rate, was applied to the SOQPSK-TG samples. Finally, AWGN samples, whose variance was defined by E_b/N_0, were added. The frame synchronizer (14) was applied to the received samples. For each value of the frequency offset and E_b/N_0, the process was repeated 10 000 times.

We now move to the question of performance measure. For linear modulations, most frame synchronizers operate on matched filter outputs sampled at 1 sample/symbol. Correctly identifying the matched filter output corresponding to the first preamble symbol is a well-defined detection event. Otherwise, a false-alarm event occurs. In contrast, the frame synchronizers in this paper operate at more than 1 sample/bit. Correspondingly, the notions of detection and false alarm are less clear. Consequently, we measure the difference between the true starting index m and its estimate $\hat{m}$. The well-established convention for assessing the performance of estimation problems such as this one is to examine the mean and variance of the estimate error. Plots of the simulated mean error are omitted here in the interest of space. The frame synchronizers with low error variance also have close-to-zero mean error. The frame synchronizers with high error variance have large mean error. For this particular problem, the mean error does not provide information (regarding the suitability of the approach to the problem) that cannot be obtained from the error variance.

The simulated estimation error variance for $\nu T_b = 0$ is plotted in Fig. 5a. The relationship between L_1 and L_2 is noteworthy. At low values of E_b/N_0, L_2 has a much lower variance than L_1, although L_2 is an approximation of L_1. As E_b/N_0 increases, the situation reverses. L_3 and L_4 have poor performance. This is because the respective approximations of L_1 and L_2 stretch the assumptions used to derive L_1 too far. L_5, L_6, and L_{6q} all have similar performance except that the variance of L_5 is about one order of magnitude lower than the variances of L_6 and L_{6q}. The variance of L_{6q} is only about two times that of L_6. Curiously, L_0 and $L_{0\rm h}$ achieve competitive estimator error variances; the variance of L_0 is near the lowest and the variance of $L_{0\rm h}$ is, for all practical purposes, the lowest. This is to be expected, given that there is no frequency offset. The fact that $L_{0\rm h}$ outperforms L_0 is why the heuristic function is popular.

Most index errors for L_0, $L_{0\rm h}$, L_1, L_2, L_5, L_6, and L_{6q} are small integer multiples of Q (the length, in samples, of the short sequences that comprise the preamble). Why this is so is illustrated by the plot in Fig. 6, which shows a plot of L_0 for the case of zero frequency offset and no noise. The iNET preamble is periodic (with period Q samples), which creates mini correlation peaks every Q samples when the occurrence of the preamble in the received samples is involved in the correlation. The highest peak corresponds to the case in which the received sample data and the preamble are aligned. The lower peaks, either side of the highest peak, correspond to cases in which fewer than eight of the preamble short sequences are aligned with the locally stored preamble template (cf. Fig. 3).

The frame synchronizer in (14) can be adjusted to look for index errors that are small integer multiples of Q. This adjustment removes these index errors. As an example, the adjustment based on looking for index errors $\pm Q$ and $\pm 2Q$ produces the estimators whose variance is plotted in Fig. 5b. Except for L_3 and L_4, this adjustment all but eliminates index errors for $E_b/N_0 > 0$ dB. There are no circle or star markers in this plot; this is because all index errors for L_0 and $L_{0\rm h}$ in Fig. 5a were either $\pm Q$ or $\pm 2Q$.

The next set of plots, shown in Fig. 7, are for $\nu T_b = 0.01$ cycles/bit. The variances of the unadjusted synchronizers are plotted in Fig. 7a and the variances of the adjusted synchronizers are plotted in Fig. 7b. The general trends are the same as before: L_3 and L_4 display unusably high index error variance, and the variance of L_1 is higher than that of L_2, L_5, L_6, and L_{6q} for low values of

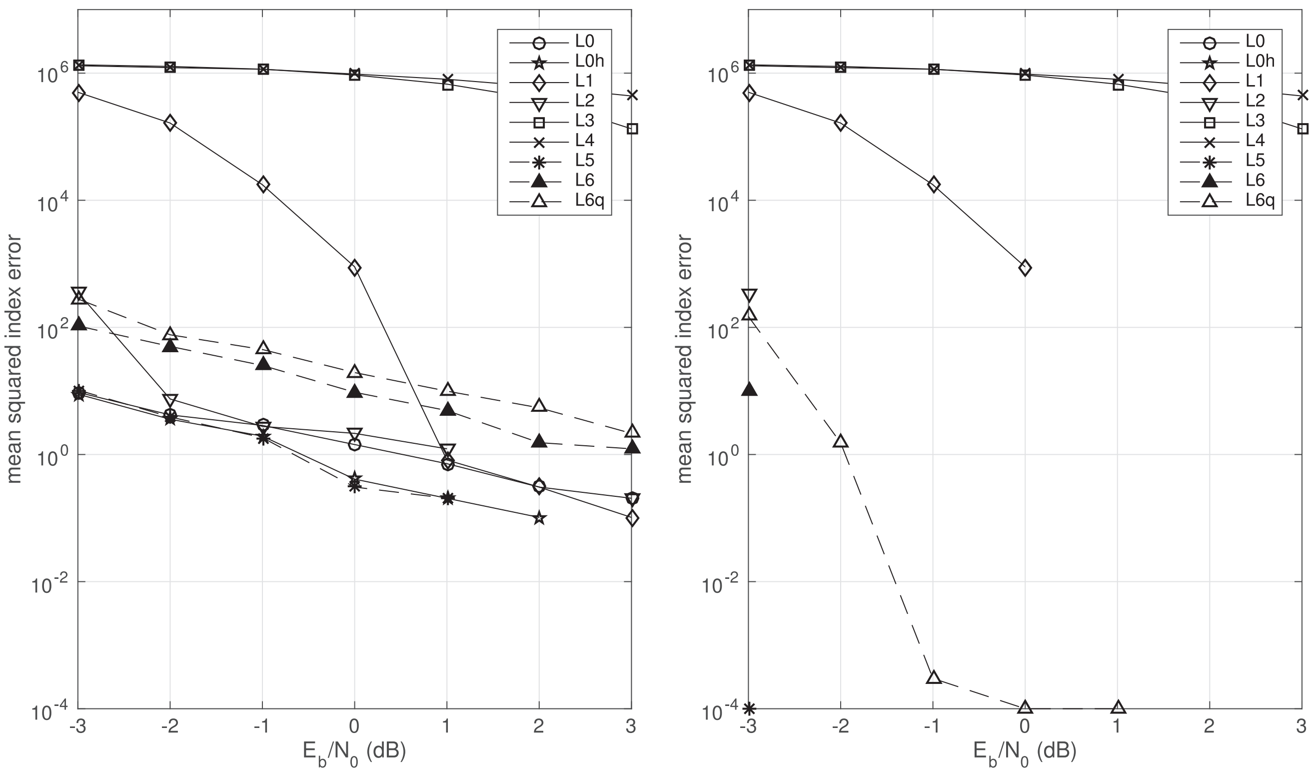

(a)

(b)

Fig. 5. Simulated mean-squared error performance for frame synchronizers described in this paper for frequency offset 0: (a) performance without adjustments, (b) performance with adjustments for errors of $\pm Q$ and $\pm 2Q$.

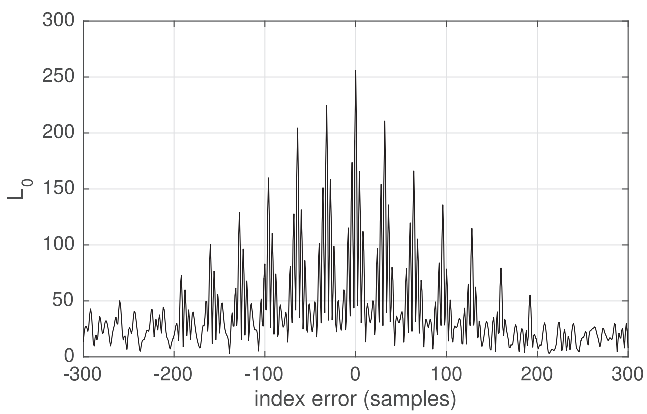

Fig. 6. Plot of $L_0(m)$ for SOQPSK-TG operating at $N = 2$ samples/bit and using iNET preamble without frequency offset and without noise.

E_b/N_0; however, the situation reverses at a higher SNR. The major difference here is that L_0 and $L_{0\text{h}}$ are quite poor. This is to be expected, because L_0 and $L_{0\text{h}}$ are not designed to account for a frequency offset.

Finally, the plots shown in Fig. 8 display the variances of the frame synchronizers for $\nu T_b = 0.05$ cycles/bit. The same trends observed in Fig. 7 are present. In this plot, the value of E_b/N_0 for which L_1 is better than L_5, L_6, and L_{6q} is lower. This is because the energy loss in L_5 and L_6 because of frequency offset (see Fig. 4) limits performance. In contrast, L_1 and L_2 were derived assuming the possibility of a larger frequency offset.

Because the simulated system operates at $N = 2$ samples/bit, an estimation error of ± 1 sample is not catastrophic; data-aided estimators see a shift by $1/2$ bit time. Consequently, any frame synchronizer that achieves an RMS index error less than 1 sample is a viable solution. The plots in Figs. 5, 7, and 8 show that for $\nu T_b \leq 0.01$ cycles/bit, the frame synchronizers L_1, L_2, L_5, L_6, and L_{6q} are capable of meeting this requirement for $E_b/N_0 > 0$ dB. Of these, Table I shows that the quantized NCPDI synchronizer L_{6q} is the best choice by a considerable margin.

The computational advantage of L_{6q} motivates further investigation. The simulated index error variance for the adjusted version of (14) based on L_{6q} as a function of the normalized frequency offset for fixed values of E_b/N_0 is plotted in Fig. 9. The performance of the unquantized version in (14) based on L_6 and the standard correlator L_0 are also plotted for reference. Using our rule of thumb that the RMS index error not exceeding 1 sample is acceptable, these plots show that as E_b/N_0 increases, the maximum frequency offset, which L_{6q} is able to tolerate also increases. For example, at $E_b/N_0 = 0$ dB, the simulation

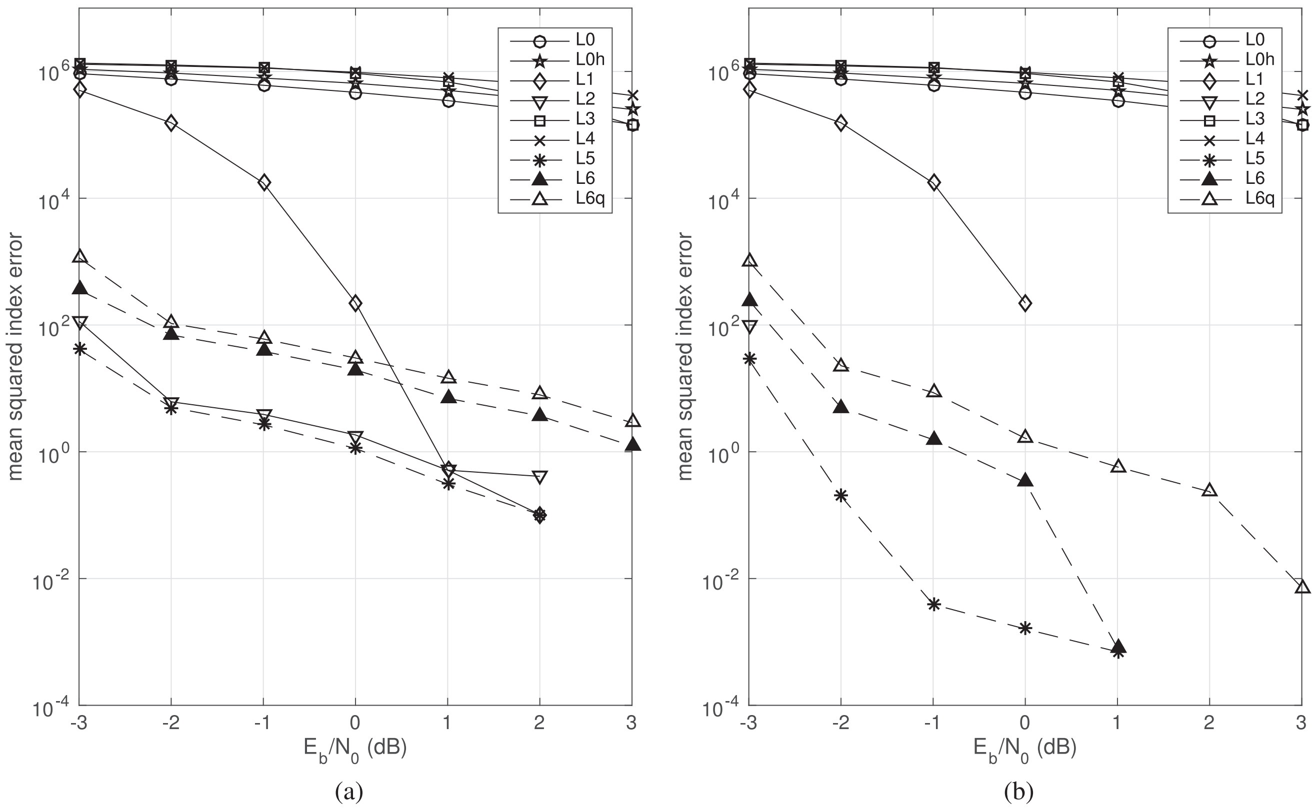

Fig. 7. Simulated mean-squared error performance for frame synchronizers described in this paper for frequency offset 1% of bit rate: (a) performance without adjustments, (b) performance with adjustments for errors of $\pm Q$ and $\pm 2Q$.

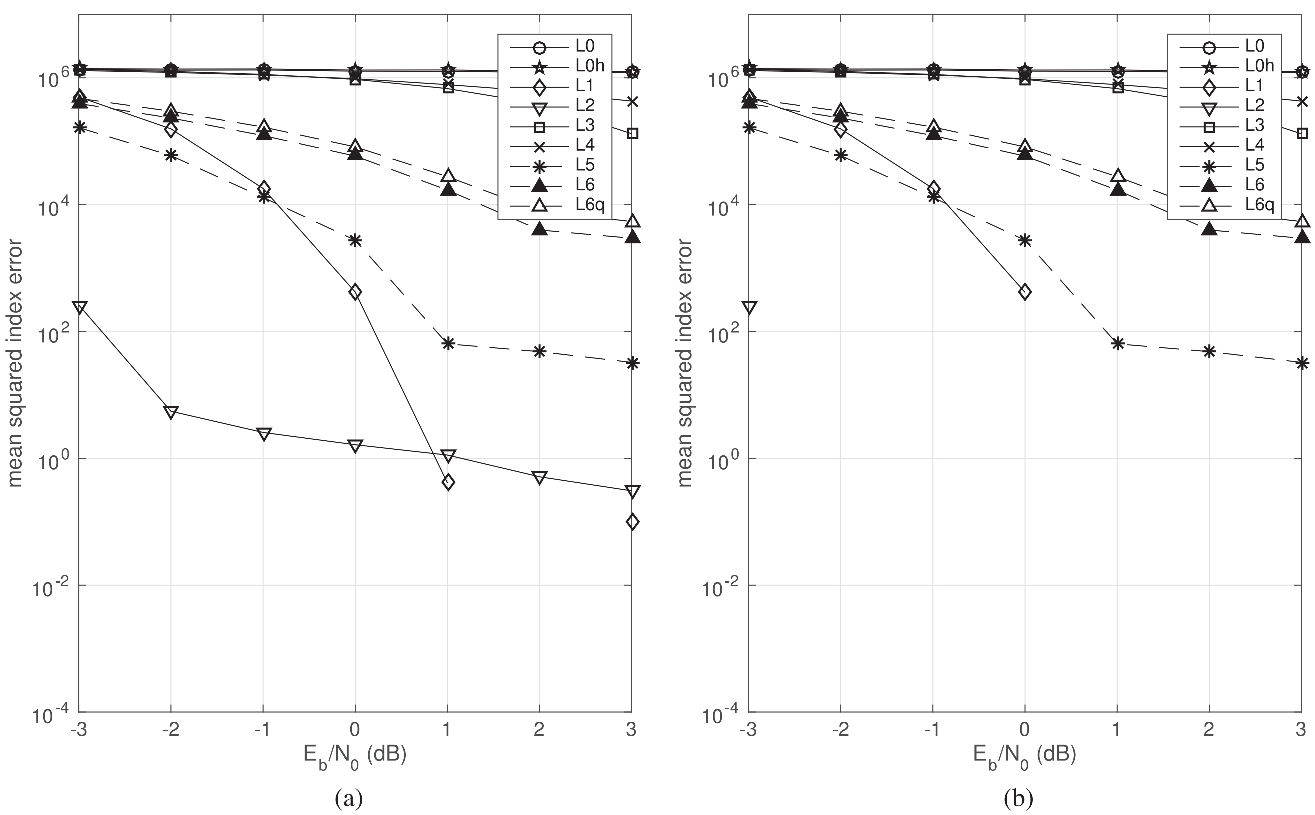

Fig. 8. Simulated mean-squared error performance for frame synchronizers described in this paper for frequency offset 5% of bit rate: (a) performance without adjustments, (b) performance with adjustments for errors of $\pm Q$ and $\pm 2Q$.

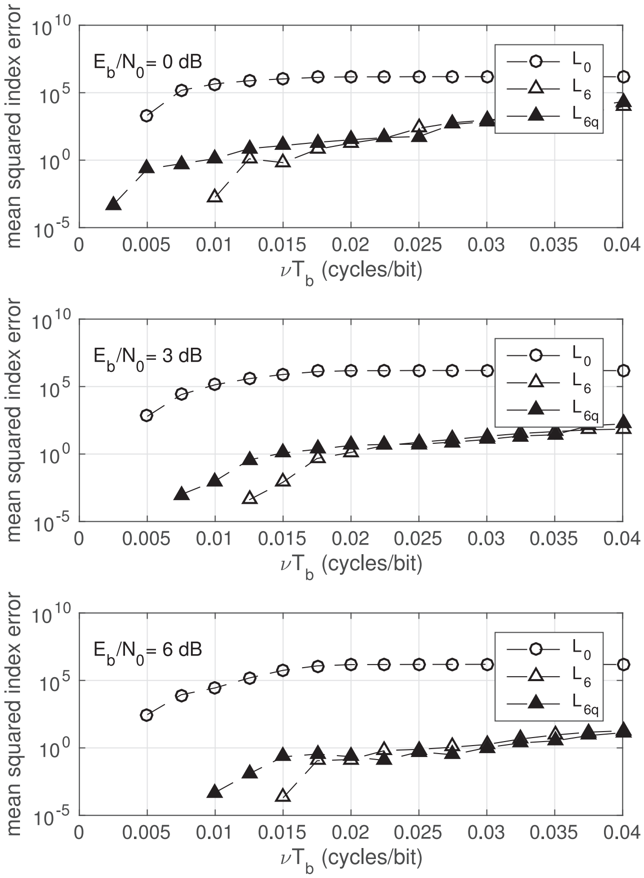

Fig. 9. Simulated index error variance for adjusted version of (14) using L_0, L_6, and L_{6q} as function of normalized frequency offset νT_b cycles/bit for three values of E_b/N_0.

results show acceptable performance for L_{6q} for $\nu T_b \leq 0.01$ cycle/bit, at $E_b/N_0 = 3$ dB for $\nu T_b \leq 0.015$ cycle/bit, and at $E_b/N_0 = 6$ dB for $\nu T_b \leq 0.03$ cycle/bit.

V. DISCUSSION AND CONCLUSIONS

By returning to basic principles, we derived ML frame synchronizers for CPM operating on samples of the received waveform, where the sampling rate satisfies the Nyquist sampling theorem. The derivation followed two approaches for dealing with the nuisance parameters: the first by Choi and Lee [9] and the second by Pedone et al. [11]. Simulation results showed that both approaches, and a number of reduced-complexity approximations, are capable of performing frame synchronization in the aeronautical telemetry environment. By leveraging the structural properties of the iNET preamble and for SOQPSK-TG operating at 2 samples/bit, low-complexity frame synchronizers with excellent performance were obtained.

The techniques outlined in this paper could be applied to any of the CPMs described in IRIG 106. As of the writing of this paper, SOQPSK-TG is the only one of the three being considered for use with the iNET preamble. Therefore, only results using SOQPSK-TG were simulated.

APPENDIX A. DERIVATION OF THE ML FRAME SYNCHRONIZER FOLLOWING CHOI AND LEE [9]

The outline and corresponding assumptions for this approach are as follows:

1) Average the likelihood function in (12) with respect to the phase θ. This step assumes the phase is uniformly distributed over the interval $[-\pi, \pi)$.

2) Average the result of the previous step with respect to the frequency offset ω. This step assumes the frequency offset is uniformly distributed over the interval $[-\pi, \pi)$.

3) Average the result of the previous step with respect to the random data. This step assumes the phase samples due to random data are independent and identically distributed random variables, each with a uniform distribution over the interval $[-\pi, \pi)$.

Assumption 2 is an approximation, because $\omega = \pi$ is equivalent to a frequency offset equal to half the sample rate. A frequency offset this high causes irreparable distortion. To see that this is so, assume the bandwidth of the continuous-time complex-valued low-pass equivalent signal is B Hz. Then, the relationship between the continuous-time frequency offset ν and the sample rate must be

$$|\nu| + B < \frac{1}{2T}. \tag{36}$$

Using $\omega = 2\pi\nu T$, the corresponding relationship for ω is

$$|\omega| < \pi\,(1 - 2BT). \tag{37}$$

Thus, any signal with $B > 0$ cannot accommodate $\omega = \pi$. Assumption 2 is made purely for mathematical convenience. The independence component of Assumption 3 is clearly not true for CPM. Independence is assumed purely in the interest of tractability. However, the uniform distribution is a good assumption for the marginal distribution of each phase sample.

The starting point is to rewrite the conditional probability density function in (12) as

$$\begin{aligned} f\,(\mathbf{r}|\,m, \theta, \omega, \phi_d) &= \frac{1}{\left(2\pi\sigma^2\right)^{F+P-1}} \exp\Bigg\{ -\frac{1}{2\sigma^2} \sum_{n=0}^{F+P-2} \Big| r\,(nT) \\ &\quad - e^{j\theta} e^{j\omega n} e^{j\phi_m(nT)} \Big|^2 \Bigg\} \end{aligned} \tag{38}$$

where the hypothesis is that the samples corresponding to the iNET preamble coincide with the received samples starting at index m. Averaging over the phase angle θ gives

$$f\,(\mathbf{r}|\,m, \omega, \phi_d) = \frac{1}{2\pi} \int_{-\pi}^{\pi} f\,(\mathbf{r}|\,m, \theta, \omega, \phi_d)\, d\theta \tag{39}$$

$$= C(\mathbf{r}) I_0 \left(\frac{1}{\sigma^2} \left| \sum_{n=0}^{F+P-2} r^*(nT) e^{j\omega n} e^{j\phi_m(nT)} \right| \right) \tag{40}$$

where

$$C(\mathbf{r}) = \frac{1}{\left(2\pi\sigma^2\right)^{F+P-1}} \exp\left\{-\frac{1}{2\sigma^2}\sum_{n=0}^{F+P-2}\left[|r(nT)|^2+1\right]\right\}. \tag{41}$$

Next, the dependency on the frequency offset ω is removed by averaging:

$$f(\mathbf{r}|\, m, \phi_d) = \frac{1}{2\pi}\int_{-\pi}^{\pi} f(\mathbf{r}|\, m, \omega, \phi_d)\, d\omega \tag{42}$$

$$= \frac{C(\mathbf{r})}{2\pi}\int_{-\pi}^{\pi} I_0\left(\frac{1}{\sigma^2}\left|\sum_{n=0}^{F+P-2} r^*(nT)\, e^{j\omega n} e^{j\phi_m(nT)}\right|\right) d\omega. \tag{43}$$

The integral is evaluated using the approximation

$$I_0(z) \approx 1 + \frac{z^2}{4} + \frac{z^4}{64}. \tag{44}$$

Thus,

$$\begin{aligned} &f(\mathbf{r}|\, m, \phi_d) \\ &\approx \frac{C(\mathbf{r})}{2\pi}\int_{-\pi}^{\pi} d\omega + \frac{C(\mathbf{r})}{16\pi^2}\int_{-\pi}^{\pi}\left|\sum_{n=0}^{F+P-2} r^*(nT)\, e^{j\omega n} e^{j\phi_m(nT)}\right|^2 d\omega \\ &\quad + \frac{C(\mathbf{r})}{1024\pi^4}\int_{-\pi}^{\pi}\left|\sum_{n=0}^{F+P-2} r^*(nT)\, e^{j\omega n} e^{j\phi_m(nT)}\right|^4 d\omega. \end{aligned} \tag{45}$$

The first integral is simply $C(\mathbf{r})$. The second and third integrals are reduced using the property

$$\int_{-\pi}^{\pi} e^{jk\omega} d\omega = \begin{cases} 2\pi & k = 0 \\ 0 & k \neq 0. \end{cases} \tag{46}$$

The second integral is

$$\begin{aligned} &\int_{-\pi}^{\pi}\left|\sum_{n=0}^{F+P-2} r^*(nT)\, e^{j\theta} e^{j\omega n} e^{j\phi_m(nT)}\right|^2 d\omega \\ &= \sum_{n_1=0}^{F+P-2}\sum_{n_2=0}^{F+P-2} r^*(n_1 T)\, r(n_2 T)\, e^{j\phi_m(n_1 T)} e^{-j\phi_m(n_2 T)} \\ &\quad \times \int_{-\pi}^{\pi} e^{j\omega n_1} e^{-j\omega n_2} d\omega \\ &= 2\pi \sum_{n=0}^{F+P-2} |r(nT)|^2. \end{aligned} \tag{47}$$

The third integral is

$$\begin{aligned} &\int_{-\pi}^{\pi}\left|\sum_{n=0}^{F+P-2} r^*(nT)\, e^{j\omega n} e^{j\phi(nT)}\right|^4 d\omega \\ &= \sum_{n_1=0}^{F+P-2}\sum_{n_2=0}^{F+P-2}\sum_{n_3=0}^{F+P-2}\sum_{n_4=0}^{F+P-2} G(m, n_1, n_2, n_3, n_4) \\ &\quad \times \int_{-\pi}^{\pi} e^{j\omega n_1} e^{-j\omega n_2} e^{j\omega n_3} e^{-j\omega n_4} d\omega \end{aligned} \tag{48}$$

where

$$\begin{aligned} &G(m, n_1, n_2, n_3, n_4) \\ &\quad = r^*(n_1 T)\, r(n_2 T)\, r^*(n_3 T)\, r(n_4 T)\, e^{j\phi_m(n_1 T)} e^{-j\phi_m(n_2 T)} \\ &\qquad \times e^{j\phi_m(n_3 T)} e^{-j\phi_m(n_4 T)}. \end{aligned} \tag{49}$$

The integral is zero except where $n_1 - \mathrm{n}_2 + n_3 - n_4 = 0$, in which case the integral evaluates to 2π. Parameterizing the nonzero condition using $i = n_1 - n_4 = n_2 - n_3$ and substituting for the integral gives

$$\begin{aligned} &\int_{-\pi}^{\pi}\left|\sum_{n=0}^{F+P-2} r^*(nT)\, e^{j\omega n} e^{j\phi_m(nT)}\right|^4 d\omega \\ &= 2\pi \sum_{n_1=0}^{F+P-2}\sum_{n_2=0}^{F+P-2} G(m, n_1, n_2, n_2, n_1) \\ &\quad + 4\pi \sum_{i=1}^{F+P-2}\sum_{n_1=i}^{F+P-2}\sum_{n_2=i}^{F+P-2} G(m, n_1, n_2, n_2 - i, n_1 - i) \\ &= 2\pi \sum_{n_1=0}^{F+P-2}\sum_{n_2=0}^{F+P-2} |r(n_1 T)|^2 |r(n_2 T)|^2 \\ &\quad + 4\pi \sum_{i=1}^{F+P-2}\sum_{n_1=i}^{F+P-2}\sum_{n_2=i}^{F+P-2} G(m, n_1, n_2, n_2 - i, n_1 - i). \end{aligned} \tag{50}$$

Assembling the results gives

$$\begin{aligned} f(\mathbf{r}|\, m, \phi_d) \approx C(\mathbf{r}) &+ \frac{C(\mathbf{r})}{8\pi}\sum_{n=0}^{F+P-2} |r(nT)|^2 \\ &+ \frac{C(\mathbf{r})}{512\pi^3}\sum_{n_1=0}^{F+P-2}\sum_{n_2=0}^{F+P-2} |r(n_1 T)|^2 |r(n_2 T)|^2 \\ &+ \frac{C(\mathbf{r})}{256\pi^3}\sum_{i=1}^{F+P-2}\sum_{n_1=i}^{F+P-2}\sum_{n_2=i}^{F+P-2} \\ &\times G(m, n_1, n_2, n_2 - i, n_1 - i). \end{aligned} \tag{51}$$

Finally, we average over the data. Here, we have

$$f(\mathbf{r}|\, m) = \int \cdots \int f(\mathbf{r}|\, m, \phi_d)\, f(\phi_d)\, d\phi_d. \tag{52}$$

The only term in (51) involving data is the fourth term, and each summand in this term contains only four signal samples. We are interested in

$$\begin{aligned} &\int \cdots \int G(m, n_1, n_2, n_2 - i, n_1 - i)\, f\left(\widetilde{\phi}\right) d\widetilde{\phi} \\ &\quad = r^*(n_1 T)\, r(n_2 T)\, r^*((n_2 - i)\, T)\, r((n_1 - i)\, T) \\ &\qquad \times I(m, i, n_1, n_2) \end{aligned} \tag{53}$$

where

$$\begin{aligned} I(m, i, n_1, n_2) = \int \cdots \int\; & e^{-j\phi_m(n_1 T)} e^{j\phi_m(n_2 T)} e^{j\phi_m((n_2 - i)T)} \\ & \times e^{-j\phi_m(n_1 - i)} f\left(\widetilde{\phi}\right) d\widetilde{\phi} \end{aligned} \tag{54}$$

and

$$\widetilde{\phi} = \left[\phi_m(n_1 T) \;\; \phi_m(n_2 T) \;\; \phi_m((n_2 - i)T) \;\; \phi_m((n_1 - i)T) \right]^\top. \tag{55}$$

When $m \leq n_1 < P + m$, $e^{j\phi_m(n_1 T)}$ is a sample corresponding to the known preamble and is treated as a constant, not a random variable. An identical situation holds for n_2, $n_2 - i$, $n_1 - i$. The integral is zero any time i, n_1, and n_2 are such that at least one sample corresponding to a random data symbol is included the integrand or except when the integrand is a constant (this occurs when $n_1 = n_2$).

It is convenient to consider the cases $i \geq P$ and $i < P$ separately. To this end, we write

$$\begin{aligned}
&\sum_{i=1}^{F+P-2} \sum_{n_1=i}^{F+P-2} \sum_{n_2=i}^{F+P-2} r^*(n_1 T)\, r(n_2 T)\, r^*((n_2 - i)T) \\
&\quad \times r((n_1 - i)T)\, I(m, i, n_1, n_2) \\
&= \sum_{i=1}^{P-1} \sum_{n_1=i}^{F+P-2} \sum_{n_2=i}^{F+P-2} r^*(n_1 T)\, r(n_2 T)\, r^*((n_2 - i)T) \\
&\quad \times r((n_1 - i)T)\, I(m, i, n_1, n_2) \\
&\quad + \sum_{i=P}^{F+P-2} \sum_{n_1=i}^{F+P-2} \sum_{n_2=i}^{F+P-2} r^*(n_1 T)\, r(n_2 T) \\
&\quad \times r^*((n_2 - i)T)\, r((n_1 - i)T)\, I(m, i, n_1, n_2).
\end{aligned} \tag{56}$$

The first term on the right-hand side of (56) represents the case in which $i < P$. For $i < P$, the integral is zero except when the following conditions are simultaneously achieved:

$$\begin{array}{ccccc}
m & \leq & n_1 & < & m + P \\
m & \leq & n_1 - i & < & m + P \\
m & \leq & n_2 & < & m + P \\
m & \leq & n_2 - i & < & m + P.
\end{array} \tag{57}$$

Because these conditions are separable, the relationship between i and n_1 and the relationship between i and n_2 may be considered separately. The relationship between i and n_1 is illustrated in Fig. 10. The two medium gray areas in the figure illustrate the constraints of the first two conditions of (57). The intersection of these constraints, shown by the dark gray region in the figure, illustrates the values of i and n_1 that produce a nonzero result. An identical relationship exists for i and n_2. Consequently, the triple summation of the first term on the right-hand side of (56) reduces to

$$\begin{aligned}
&\sum_{i=1}^{P-1} \sum_{n_1=i}^{F+P-2} \sum_{n_2=i}^{F+P-2} r^*(n_1 T)\, r(n_2 T) \\
&\times r^*((n_2 - i)T)\, r((n_1 - i)T)\, I(m, i, n_1, n_2) \\
&= \sum_{i=1}^{P-1} \left[\sum_{n_1=i+m}^{m+P-1} r^*(n_1 T) e^{j\phi_m(n_1 T)} r((n_1 - i)T)\, e^{-j\phi_m((n_1 - i)T)} \right. \\
&\quad \left. \times \sum_{n_2=i+m}^{m+P-1} r(n_2 T)\, e^{-j\phi_m(n_2 T)} r^*((n_2 - i)T)\, e^{j\phi_m((n_2 - i)T)} \right] \\
&= \sum_{i=1}^{P-1} \left| \sum_{n=i+m}^{m+P-1} r^*(nT)\, e^{j\phi_m(nT)} r((n - i)T)\, e^{-j\phi_m((n-i)T)} \right|^2.
\end{aligned} \tag{58}$$

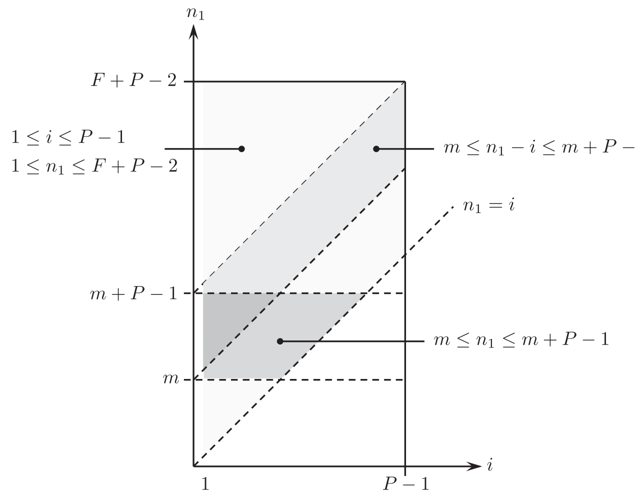

Fig. 10. Relationship of indexes involved in summations in (56) [cf. (57)].

The second term on the right-hand side of (56) represents the case in which $i \geq P$. Here, one of the elements of $\widetilde{\phi}$ is guaranteed to be a sample corresponding to a random data symbol. Consequently, the integral is zero except when $n_1 = n_2$:

$$I(m, i, n_1, n_2) = \begin{cases} 0 & n_1 \neq n_2 \\ 1 & n_1 = n_2. \end{cases} \tag{59}$$

The triple summation of the second term on the right-hand side of (56) reduces to

$$\begin{aligned}
&\sum_{i=P}^{F+P-2} \sum_{n_1=i}^{F+P-2} \sum_{n_2=i}^{F+P-2} r^*(n_1 T)\, r(n_2 T) \\
&\times r^*((n_2 - i)T)\, r((n_1 - i)T)\, I(m, i, n_1, n_2) \\
&= \sum_{i=P}^{F+P-2} \sum_{n=i}^{F+P-2} |r(nT)|^2 |r((n - i)T)|^2.
\end{aligned} \tag{60}$$

The double summation represents all correlations of samples corresponding to random data symbols. Adding and subtracting the double summation for all correlations of samples involving only samples corresponding to preamble symbols gives

$$\begin{aligned}
&\sum_{i=P}^{F+P-2} \sum_{n=i}^{F+P-2} |r(nT)|^2 |r((n - i)T)|^2 \\
&\quad = \sum_{i=1}^{F+P-2} \sum_{n=i}^{F+P-2} |r(nT)|^2 |r((n - i)T)|^2
\end{aligned}$$

$$-\sum_{i=1}^{P-1}\sum_{n=i+m}^{m+P-1}|r(nT)|^2|r((n-i)T)|^2. \quad (61)$$

Assembling these results gives

$$\begin{aligned}
&f(\mathbf{r}|m)\\
&\approx \frac{C(\mathbf{r})}{8\pi}+2\pi\sum_{n=0}^{F+P-2}|r(nT)|^2\\
&+\frac{C(\mathbf{r})}{512\pi^3}\sum_{n_1=0}^{F+P-2}\sum_{n_2=0}^{F+P-2}|r(n_1T)|^2|r(n_2T)|^2+\frac{C(\mathbf{r})}{256\pi^3}\\
&\times\sum_{i=1}^{P-1}\left|\sum_{n=i+m}^{m+P-1}r^*(nT)e^{j\phi_m(nT)}r((n-i)T)e^{-j\phi_m((n-i)T)}\right|^2\\
&+\frac{C(\mathbf{r})}{256\pi^3}\sum_{i=1}^{F+P-2}\sum_{n=i}^{F+P-2}|r(nT)|^2|r((n-i)T)|^2\\
&-\frac{C(\mathbf{r})}{256\pi^3}\sum_{i=1}^{P-1}\sum_{n=i+m}^{m+P-1}|r(nT)|^2|r((n-i)T)|^2. \quad (62)
\end{aligned}$$

Eliminating terms that do not depend on m and using the change of variables $k=n-m$ gives

$$\begin{aligned}
L'_1(m)=\sum_{i=1}^{P-1}\Bigg|\sum_{k=i}^{P-1}&r^*((k+m)T)e^{j\phi_m((k+m)T)}\\
&\times r((k+m-i)T)e^{-j\phi_m((k+m-i)T)}\Bigg|^2\\
&-\sum_{i=1}^{P-1}\sum_{n=i+m}^{m+P-1}|r(nT)|^2|r((n-i)T)|^2. \quad (63)
\end{aligned}$$

The function $L'_1(m)$ is unbalanced [9]; that is, $L'_1(m)\neq 0$ in the noise-free case, where m is the true starting index of the preamble sequence. As explained in [9], a balanced function is obtained from $L'_1(m)$ by removing the squares applied to the summands in (63) to produce

$$\begin{aligned}
L_1(m)=\sum_{i=1}^{P-1}\Bigg|\sum_{k=i}^{P-1}&r^*((k+m)T)e^{j\phi_m((k+m)T)}\\
&\times r((k+m-i)T)e^{-j\phi_m((k+m-i)T)}\Bigg|\\
&-\sum_{i=1}^{P-1}\sum_{n=i+m}^{m+P-1}|r(nT)|\,|r((n-i)T)|. \quad (64)
\end{aligned}$$

Finally, using the relationship $p(k)=e^{j\phi_m((k+m)T)}$ gives the form for $L_1(m)$ given by (17).

APPENDIX B. DERIVATION OF THE ML FRAME SYNCHRONIZER FOLLOWING PEDONE ET AL. [11]

The outline and corresponding assumptions for this approach are as follows:

1) Average the likelihood function in (12) with respect to the random data. This step assumes the phase samples due to random data are independent and identically distributed random variables, each with a uniform distribution over the interval $[-\pi,\pi)$.

2) Average the result of the previous step with respect to the phase θ. This step assumes the phase is uniformly distributed over the interval $[-\pi,\pi)$.

3) Compute the logarithm of the previous step. This produces a log-likelihood function for m and ω.

4) Estimate ω using some simplifying assumptions, and substitute the estimate into the previous step.

The independence component of Assumption 1 is clearly not true for CPM. Independence is assumed purely in the interest of tractability. However, the uniform distribution is a good assumption for the marginal distribution of each phase sample.

Expanding the squares in the exponents of the conditional probability density function in (12) and partitioning the product into three products corresponding to samples produced by random data and samples produced by the pilot symbols gives

$$\begin{aligned}
&f(\mathbf{r}|m,\theta,\omega,\phi_d)\\
&=C(\mathbf{r})\prod_{n=0}^{m-1}\exp\left\{\frac{1}{\sigma^2}\mathrm{Re}\left[r(nT)e^{-j\theta}e^{-j\omega n}e^{-j\phi_m(nT)}\right]\right\}\\
&\quad\times\prod_{n=m}^{m+P-1}\exp\left\{\frac{1}{\sigma^2}\mathrm{Re}\left[r(nT)e^{-j\theta}e^{-j\omega n}e^{-j\phi_m(nT)}\right]\right\}\\
&\quad\times\prod_{n=m+P}^{F+P-2}\exp\left\{\frac{1}{\sigma^2}\mathrm{Re}\left[r(nT)e^{-j\theta}e^{-j\omega n}e^{-j\phi_m(nT)}\right]\right\}
\end{aligned} \quad (65)$$

where $C(\mathbf{r})$ is given by (41).

The first step is to average with respect to the data:

$$f(\mathbf{r}|m,\theta,\omega)=\int\cdots\int f(\mathbf{r}|m,\theta,\omega,\phi_d)\,f(\phi_d)\,d\phi_d \quad (66)$$

Because the phase samples due to random data are assumed to be independent uniformly distributed random variables,

$$f(\phi_d)=\prod_{n=0}^{m-1}f(\phi(nT))\prod_{n=m+P}^{F+P-2}f(\phi(nT)) \quad (67)$$

where

$$f(\phi(nT))=\begin{cases}\frac{1}{2\pi} & -\pi\le\phi(nT)<\pi\\ 0 & \text{otherwise.}\end{cases} \quad (68)$$

Consequently, we have

$$\begin{aligned}
&f(\mathbf{r}|m,\theta,\omega)\\
&=C(\mathbf{r})\prod_{n=0}^{m-1}\frac{1}{2\pi}\int_{-\pi}^{\pi}\exp\left\{\frac{1}{\sigma^2}\mathrm{Re}\left[r(nT)e^{-j\theta}e^{-j\omega n}e^{-j\alpha}\right]\right\}d\alpha\\
&\quad\times\prod_{n=m+P}^{F+P-2}\frac{1}{2\pi}\int_{-\pi}^{\pi}\exp\left\{\frac{1}{\sigma^2}\mathrm{Re}\left[r(nT)e^{-j\theta}e^{-j\omega n}e^{-j\alpha}\right]\right\}d\alpha
\end{aligned}$$

$$\times \prod_{n=m}^{m+P-1} \exp\left\{\frac{1}{\sigma^2}\mathrm{Re}\left[r(nT)e^{-j\theta}e^{-j\omega n}e^{-j\phi_m(nT)}\right]\right\} \quad (69)$$

which leads to

$$\begin{aligned} f(\mathbf{r}|\, m,\theta,\omega) &= C(\mathbf{r})\prod_{n=0}^{m-1} I_0\left(\frac{1}{\sigma^2}|r(nT)|\right)\prod_{n=m+P}^{F+P-2} I_0\left(\frac{1}{\sigma^2}|r(nT)|\right) \\ &\times \prod_{n=m}^{m+P-1}\exp\left\{\frac{1}{\sigma^2}\mathrm{Re}\left[r(nT)e^{-j\theta}e^{-j\omega n}e^{-j\phi_m(nT)}\right]\right\}. \end{aligned} \quad (70)$$

The next step is to average over the phase. This gives

$$\begin{aligned} f(\mathbf{r}|\, m,\omega) &= \frac{1}{2\pi}\int_{-\pi}^{\pi} f(\mathbf{r}|\, m,\theta,\omega)\,d\theta \\ &= C(\mathbf{r})\prod_{n=0}^{m-1} I_0\left(\frac{1}{\sigma^2}|r(nT)|\right)\prod_{n=m+P}^{F+P-2} I_0\left(\frac{1}{\sigma^2}|r(nT)|\right) \\ &\times \frac{1}{2\pi}\int_{-\pi}^{\pi}\exp\left\{e^{j\theta}\frac{1}{\sigma^2}\sum_{n=m}^{m+P-1}\mathrm{Re}\left[r(nT)e^{-j\omega n}e^{-j\phi_m(nT)}\right]\right\}d\theta \end{aligned} \quad (71)$$

which evaluates to

$$\begin{aligned} f(\mathbf{r}|\, m,\omega) &= C(\mathbf{r})\prod_{n=0}^{m-1} I_0\left(\frac{1}{\sigma^2}|r(nT)|\right)\prod_{n=m+P}^{F+P-2} I_0\left(\frac{1}{\sigma^2}|r(nT)|\right) \\ &\times I_0\left(\frac{1}{\sigma^2}\left|\sum_{n=m}^{m+P-1} r(nT)e^{-j\omega n}e^{-j\phi_m(nT)}\right|\right). \end{aligned} \quad (72)$$

The log-likelihood function is obtained by computing the logarithm of the conditional probability density function in (72). Dropping the scale constant that is not a function of m gives

$$\begin{aligned} \Lambda''(m,\omega) &= \sum_{n\in\mathcal{D}_m}\log\left\{I_0\left(\frac{1}{\sigma^2}|r(nT)|\right)\right\} \\ &+ \log\left\{I_0\left(\frac{1}{\sigma^2}\left|\sum_{n=m}^{m+P-1} r(nT)e^{-j\omega n}e^{-j\phi_m(nT)}\right|\right)\right\} \end{aligned} \quad (73)$$

where $\mathcal{D}_m$ is the set of indexes of samples corresponding to random data:

$$\mathcal{D}_m = \{0,\ldots,m-1\}\cup\{m+P,\ldots,F+P-2\}. \quad (74)$$

Rewrite the first term as

$$\begin{aligned} \sum_{n\in\mathcal{D}_m}&\log\left\{I_0\left(\frac{1}{\sigma^2}|r(nT)|\right)\right\} \\ &= \sum_{n\in\mathcal{D}_m}\log\left\{I_0\left(\frac{1}{\sigma^2}|r(nT)|\right)\right\} \\ &+ \sum_{n=m}^{m+P-1}\log\left\{I_0\left(\frac{1}{\sigma^2}|r(nT)|\right)\right\} \\ &- \sum_{n=m}^{m+P-1}\log\left\{I_0\left(\frac{1}{\sigma^2}|r(nT)|\right)\right\} \\ &= \sum_{n=0}^{F+P-2}\log\left\{I_0\left(\frac{1}{\sigma^2}|r(nT)|\right)\right\} \\ &- \sum_{n=m}^{m+P-1}\log\left\{I_0\left(\frac{1}{\sigma^2}|r(nT)|\right)\right\}. \end{aligned} \quad (75)$$

Recognizing the first term is not a function of m and may be dropped, the log-likelihood function becomes

$$\begin{aligned} \Lambda'(m,\omega) &= \log\left\{I_0\left(\frac{1}{\sigma^2}\left|\sum_{n=m}^{m+P-1} r(nT)e^{-j\omega n}e^{-j\phi_m(nT)}\right|\right)\right\} \\ &- \sum_{n=m}^{m+P-1}\log\left\{I_0\left(\frac{1}{\sigma^2}|r(nT)|\right)\right\}. \end{aligned} \quad (76)$$

Following Pedone et al. [11], the frequency offset is treated as a nuisance parameter whose estimate is used to produce a log-likelihood function for m. Because the first term on the right-hand side of (76) is the only one containing ω, the starting point is the correlation in the argument of the Bessel function:

$$\varrho = \sum_{n=m}^{m+P-1} r(nT)e^{-j\phi_m(nT)}e^{-j\omega n} \quad (77)$$

$$= e^{j\omega m}\sum_{k=0}^{P-1} r((k+m)T)e^{-j\phi_m((k+m)T)}e^{-j\omega k}. \quad (78)$$

Now, partition the length-P summation over n using $P = L_{\mathrm{PDI}}\, L_{\mathrm{coh}}$. This partitions the correlation sum into $L_{\mathrm{PDI}} = P/L_{\mathrm{coh}}$ nonoverlapping segments, each of length L_{coh}:

$$\varrho = e^{j\omega m}\sum_{k'=0}^{L_{\mathrm{PDI}}}\sum_{k=k'L_{\mathrm{coh}}}^{(k'+1)L_{\mathrm{coh}}-1} r((k+m)T)e^{-j\phi_m((k+m)T)}e^{-j\omega k}. \quad (79)$$

If the ω and L_{coh} are such that $e^{-j\omega k}\approx e^{-j\omega k' L_{\mathrm{coh}}}$ for $k = k'L_{\mathrm{coh}},\ldots,(k'+1)L_{\mathrm{coh}}-1$, then ϱ may be rewritten as

$$\begin{aligned} \varrho &= e^{j\omega m}\sum_{k'=0}^{L_{\mathrm{PDI}}} e^{-j\omega k' L_{\mathrm{coh}}} \\ &\times \underbrace{\sum_{k=k'L_{\mathrm{coh}}}^{(k'+1)L_{\mathrm{coh}}-1} r((k+m)T)e^{-j\phi_m((k+m)T)}}_{\rho(m,k')} \end{aligned} \quad (80)$$

from which we have

$$|\varrho|^2 = \sum_{k_1=0}^{L_{\mathrm{PDI}}-1}\sum_{k_2=0}^{L_{\mathrm{PDI}}-1} e^{-j\omega k_1 L_{\mathrm{coh}}}e^{j\omega k_2 L_{\mathrm{coh}}}\rho(m,k_1)\rho^*(m,k_2). \quad (81)$$

Rearranging the double summation along the diagonal lines $k_2 = k_1 + n$ organizes the correlations in terms of delay n. The result is

$$|\varrho|^2 = \sum_{n=-L_{\mathrm{PDI}}+1}^{-1} e^{-j\omega n L_{\mathrm{coh}}} \sum_{i=0}^{L_{\mathrm{PDI}}-1-n} \rho(m, i+n)\rho^*(m, i) + \sum_{i=0}^{L_{\mathrm{PDI}}-1} |\rho(m,i)|^2 + \sum_{n=1}^{L_{\mathrm{PDI}}-1} e^{j\omega n L_{\mathrm{coh}}} \sum_{i=0}^{L_{\mathrm{PDI}}-1-n} \rho(m,i)\rho^*(m,i+n) \tag{82}$$

$$= \sum_{i=0}^{L_{\mathrm{PDI}}-1} |\rho(m,i)|^2 + \sum_{n=1}^{L_{\mathrm{PDI}}-1} 2\mathrm{Re}\left\{ e^{-j\omega n L_{\mathrm{coh}}} \sum_{i=0}^{L_{\mathrm{PDI}}-1-n} \rho^*(m,i)\rho(m,i+n) \right\} \tag{83}$$

$$= \Lambda_0(m) + \sum_{n=1}^{L_{\mathrm{PDI}}-1} \Lambda_n(m,\omega). \tag{84}$$

Here, $\Lambda_n(m, \omega)$ is interpreted as an n-delay correlation of $\rho(m, i)$, followed by a phase rotation proportional to ω. When $n = 0$, the phase rotation term is not present and $\Lambda_0(m)$ corresponds to NCPDI [11].

Maximizing the second term with respect to ω is intractably difficult. Instead, Pedone et al. [11] develop the notion of maximizing each summand with respect to ω. This produces a sequence of frequency offset estimates:

$$\hat{\omega}_n = \frac{\arg\left\{ \sum_{i=0}^{L_{\mathrm{PDI}}-1-n} \rho(m,i+n)\rho^*(m,i) \right\}}{n L_{\mathrm{coh}}}. \tag{85}$$

These estimates are used to remove the dependency on ω from (76). Using the relationship

$$e^{j\hat{\omega}_n n L_{\mathrm{coh}}} = \frac{\sum_{i=0}^{L_{\mathrm{PDI}}-1-n} \rho(m,i+n)\rho^*(m,i)}{\left| \sum_{i=0}^{L_{\mathrm{PDI}}-1-n} \rho(m,i+n)\rho^*(m,i) \right|} \tag{86}$$

we have

$$\bar{\Lambda}_n(m) = \Lambda_n(m, \hat{\omega}_n) \tag{87}$$

$$= 2\mathrm{Re}\left\{ e^{-j\hat{\omega} n L_{\mathrm{coh}}} \sum_{i=0}^{L_{\mathrm{PDI}}-1-n} \rho(m,i+n)\rho^*(m,i) \right\} \tag{88}$$

$$= 2\mathrm{Re}\left\{ \frac{\left(\sum_{i=0}^{L_{\mathrm{PDI}}-1-n} \rho(m,i+n)\rho^*(m,i) \right)^*}{\left| \sum_{i=0}^{L_{\mathrm{PDI}}-1-n} \rho(m,i+n)\rho^*(m,i) \right|} \times \sum_{i=0}^{L_{\mathrm{PDI}}-1-n} \rho(m,i+n)\rho^*(m,i) \right\} \tag{89}$$

$$= 2\left| \sum_{i=0}^{L_{\mathrm{PDI}}-1-n} \rho(m,i+n)\rho^*(m,i) \right|. \tag{90}$$

$\bar{\Lambda}_n(m)$ is called n-span DPDI [11].

The correlation ϱ may be expressed as

$$\varrho = \sqrt{\Lambda_0(m) + \sum_{n=1}^{L_{\mathrm{PDI}}-1} \bar{\Lambda}_n(m)}. \tag{91}$$

Inserting these results into the log-likelihood function in (76) gives

$$\Lambda(m) = \log\left\{ I_0\left(\frac{1}{\sigma^2} \sqrt{\Lambda_0(m) + \sum_{n=1}^{L_{\mathrm{PDI}}-1} \bar{\Lambda}_n(m)} \right) \right\} - \sum_{n=m}^{m+P-1} \log\left\{ I_0\left(\frac{1}{\sigma^2} |r(nT)| \right) \right\}. \tag{92}$$

The high SNR approximation based on $I_0(z) \approx e^z$ is

$$L_5(m) \approx \sqrt{\Lambda_0(m) + \sum_{n=1}^{L_{\mathrm{PDI}}-1} \bar{\Lambda}_n(m)} - \sum_{n=m}^{m+P-1} |r(nT)| \tag{93}$$

given by (21) in the main body.

REFERENCES

[1] Radio access network (RAN) standard. Version 0.7.9. Integrated Network Enhanced Telemetry (iNET) Radio Access Network Standards Working Group, 3 December 2012. [Online]. https://www.tena-sda.org/display/INET/iNET + Platform + Interface + Standards.

[2] Barker, R. H. Group synchronization of binary digital systems. In *Communication Theory*, W. Jackson, Ed. London, United Kingdom: Butterworth, 1953, pp. 273–287.

[3] Massey, J. Optimum frame synchronization. *IEEE Transactions on Communications*, **20**, 2 (Apr. 1972), 115–119.

[4] Nielsen, P. T. Some optimum, and suboptimum frame synchronizers for binary data in Gaussian noise. *IEEE Transactions on Communications*, **21**, 6 (June 1973), 770–772.

[5] Chiani, M. Noncoherent frame synchronization. *IEEE Transactions on Communications*, **58**, 5 (May 2010), 1536–1545.

[6] Lui, G., and Tan, H. Frame synchronization for Gaussian channels. *IEEE Transactions on Communications*, **35**, 8 (Aug. 1987), 818–829.

[7] Chiani, M., and Martini, M. Analysis of optimum frame synchronization based on periodically embedded sync words.

IEEE Transactions on Communications, **55**, 11 (Nov. 2007), 2056–2060.

[8] Bastaki, E., Tan, H., Shi, Y., and Letaief, K. B. Frame synchronization based on multiple frame observations. *IEEE Transactions on Wireless Communications*, **9**, 3 (Mar. 2010), 1097–1107.

[9] Choi, Z., and Lee, Y. Frame synchronization in the presence of frequency offset. *IEEE Transactions on Communications*, **50**, 7 (July 2002), 1062–1065.

[10] Koo, Y., and Lee, Y. A joint maximum likelihood approach to frame synchronization in presence of frequency offset. In *Proceedings of the IEEE International Conference on Communications*, New York, 28 Apr.–2 May 2002, 1546–1550.

[11] Pedone, R., Villanti, M., Vanelli-Coralli, A., Corazza, G., and Mathiopoulos, P. T. Frame synchronization in frequency uncertainty. *IEEE Transactions on Communications*, **58**, 4 (Apr. 2010), 1235–1246.

[12] Mehlan, R., and Meyr, H. Optimum frame synchronization for asynchronous packet transmission. In *Proceedings of the IEEE International Conference on Communications*, Geneva, Switzerland, 23–26 May 1993, 826–830.

[13] Chiani, M., and Martini, M. Practical frame synchronization for data with unknown distribution on AWGN channels. *IEEE Communications Letters*, **9**, 5 (May 2005), 456–458.

[14] Chiani, M., and Martini, M. On sequential frame synchronization in AWGN channels. *IEEE Transactions on Communications*, **54**, 2 (Feb. 2006), 339–348.

[15] Gansman, J., Fitz, M., and Krogmeier, J. Optimum, and suboptimum frame synchronization for pilot-symbol-assisted modulation. *IEEE Transactions on Communications*, **45**, 10 (Oct. 1997), 1327–1337.

[16] van Wijngaarden, A., and Willink, T. Frame synchronization using distributed sequences. *IEEE Transactions on Communications*, **48**, 12 (Dec. 2000), 2127–2138.

[17] Stantchev, B., and Fettweis, G. Optimum frame synchronization for orthogonal FSK in flat fading channels, and one burst application. In *Proceedings of the IEEE Wireless Communications and Networking Conference*, New Orleans, LA, 21–24 Sept. 1999, 1070–1074.

[18] Bobula, M., Daněk, K., and Prokeš, A. Simplified frame, and symbol synchronization for 4CPFSK with $h = 0.25$. *Radioengineering*, **17**, 2 (June 2008), 108–114.

[19] Huh, H., and Krogmeier, J. A unified approach to optimum frame synchronization. *IEEE Transactions on Wireless Communications*, **5**, 12 (Dec. 2006), 3700–3711.

[20] Hosseini, E., and Perrins, E. Timing, carrier, and frame synchronization of burst-mode CPM. *IEEE Transactions on Communications*, **61**, 12 (Dec. 2013), 5125–5138.

[21] Hosseini, E., and Perrins, E. The Cramér-Rao bound for training sequence design for burst-mode CPM. *IEEE Transactions on Communications*, **61**, 6 (June 2013), 2396–2407.

[22] Rice, M., McMurdie, A., and Perrins, E. A low-complexity preamble detector for iNET-formatted SOQPSK. In *Proceedings of the IEEE Military Communications Conference*, Oct. 2014, 718–723.

[23] Aulin, T., Rydbeck, N., and Sundberg, C.-E. Continuous phase modulation—Part I: Full response signaling. *IEEE Transactions on Communications*, **29**, 3 (Mar. 1981), 196–209.

[24] Aulin, T., Rydbeck, N., and Sundberg, C.-E. Continuous phase modulation—Part II: Partial response signaling. *IEEE Transactions on Communications*, **29**, 3 (Mar. 1981), 210–225.

[25] Anderson, J. B., Aulin, T., and Sundberg, C.-E. *Digital Phase Modulation*. New York: Plenum Press, 1986.

[26] Telemetry Standards. IRIG standard 106-04, Range Commanders Council Telemetry Group, Range Commanders Council, White Sands Missile Range, NM, 2004. [Online]. http://www.wsmr.army.mil/RCCsite/Pages/Publications.aspx.

[27] Perrins, E., and Rice, M. Reduced-complexity approach to iterative detection of coded SOQPSK. *IEEE Transactions on Communications*, **55** (July 2007), 1354–1362.

[28] Nelson, T., Perrins, E., and Rice, M. Near optimal common detection techniques for shaped offset QPSK, and Feher's QPSK. *IEEE Transactions on Communications*, **56** (May 2008), 724–735.

[29] Simon, M., Omura, J., Scholtz, R., and Levitt, B. *Spread Spectrum Communications Handbook*, electronic ed. New York: McGraw-Hill, 2002.

[30] Viterbi, A. *CDMA: Principles of Spread Spectrum Communication.* Reading, MA: Addison-Wesley, 1995.

[31] Corazza, G., Pedone, R., and Villanti, M. Frame acquisition for continuous and discontinuous transmission in the forward link of Ka-band satellite systems. *International Journal of Satellite Communications and Networking*, **24**, 2 (Mar./Apr. 2006), 185–201.

Michael Rice (M'82—SM'98) received a B.S.E.E. degree from Louisiana Tech University in 1987 and his Ph.D. degree from Georgia Tech in 1991. Dr. Rice was with Digital Transmission Systems in Atlanta and joined the faculty at Brigham Young University in 1991, where he is the Jim Abrams Professor in the Department of Electrical and Computer Engineering. Professor Rice was a National Aeronautics and Space Administration/American Society for Engineering Education Summer faculty fellow at the Jet Propulsion Laboratory during 1994 and 1995, where he worked on land mobile satellite systems. During the 1999–2000 academic year, Professor Rice was a visiting scholar at the Communication Systems and Signal Processing Institute at San Diego State University.

Professor Rice's research interests are in the areas of digital communication theory and error control coding, with a special interest in applications to aeronautical telemetering and software radio design. He has been a consultant to both government and industry on telemetry-related issues and serves as an associate member of the Telemetry Group of the Range Commander's Council. He is a member of the Institute of Electrical and Electronics Engineers (IEEE) Communications Society and is past chair of the Communication Theory Technical Committee. He is the technical editor for *Command, Control and Communication Systems* and an associate editor in chief for *IEEE Transactions on Aerospace and Electronic Systems.* He was elected to the Aerospace and Electronic Systems Society board of governors for the 2016–2018 term.

Andrew McMurdie studied electrical engineering at Brigham Young University, receiving his B.S.E.E. degree in 2013 and M.S.E.E. degree in 2015. His research focus areas were signal processing and digital communications. In 2015, Andrew joined Raytheon Missile System's signal processing department, where he now works on various communication and radar systems.